Thermal Decomposition of Ethylene Oxide: Potential Energy Surface, Master Equation Analysis, and Detailed Kinetic Modeling

Ameya Joshi,[†] Xiaoqing You,[‡] Timothy A. Barckholtz,*[,§] and Hai Wang*[,‡]

Department of Mechanical Engineering, University of Delaware, Newark, Delaware 19711, Department of Aerospace and Mechanical Engineering, University of Southern California, Los Angeles, California 90089, and Corporate Strategic Research, ExxonMobil Research and Engineering Company, Annandale, New Jersey 08801

Received: March 31, 2005; In Final Form: June 15, 2005

The unimolecular decomposition of ethylene oxide (oxirane) and the oxiranyl radial is examined by molecular orbital calculations, Rice−Ramsperger−Kassel−Marcus (RRKM)/Master Equation analysis, and detailed kinetic modeling of ethylene oxide pyrolysis in a single-pulse shock tube. It was found that the largest energy barrier to the decomposition of ethylene oxide lies in its initial isomerization to form acetaldehyde, and in agreement with previous studies, the isomerization was found to proceed through the $^{\bullet}CH_2CH_2O^{\bullet}$ biradical. Because of the biradical nature of the transition states and intermediate, the energy barriers for the initial C−O rupture in ethylene oxide and the subsequent 1,2-H shift remain highly uncertain. An overall isomerization energy barrier of 59 ± 2 kcal/mol was found to satisfactorily explain the available single pulse shock tube data. This barrier height is in line with the estimates made from an approximate spin-corrected procedure at the MP4/6-31+G(d) and QCISD(T)/6-31G(d) levels of theory. The dominant channel for the unimolecular decomposition of ethylene oxide was found to form CH_3 + HCO at around the ambient pressure. It accounts for >90% of the total rate constant for $T > 800$ K. The high-pressure limit rate constant for the unimolecular decomposition of ethylene oxide was calculated as $k_{1,\infty}(s^{-1}) = (3.74 \times 10^{10})T^{1.298}e^{-29990/T}$ for $600 < T < 2000$ K.

Introduction

The unimolecular isomerization and decomposition of ethylene oxide (c-C_2H_4O, oxirane) have been subject to extensive

$$c\text{-}C_2H_4O \rightarrow \text{products} \qquad \text{(R1)}$$

experimental and theoretical studies. Early work[1−7] discussed the mechanism of the first reaction steps in the decomposition of ethylene oxide. Lifshitz et al.[8] studied the pyrolysis of ethylene oxide in a single pulse shock tube between 830 and 1200 K and 1.5−10 atm. Major products observed include ethane, ethylene, methane, acetylene, acetaldehyde, propane, and hydrogen. A kinetic mechanism, consisting of 18 elementary steps, was proposed and includes the following unimolecular reactions for the decomposition of ethylene oxide,

$$c\text{-}C_2H_4O \rightarrow CH_3CHO \qquad \text{(R1a)}$$

$$\rightarrow CH_3 + HCO \qquad \text{(R1b)}$$

$$\rightarrow CH_4 + CO \qquad \text{(R1c)}$$

Lifshitz and co-workers assigned a total rate constant

$$k_1\,(s^{-1}) = (1.21 \times 10^{14})e^{-57.2(\text{kcal/mol})/RT}$$

with $k_{1a} \sim 0.6k_1$ and $k_{1b} \sim 0.3k_1$. They were able to reproduce most of the species concentrations after a 2 ms dwell time over the entire range of temperature considered in the experiment. In addition, the species concentrations were found to be independent of total pressure, suggesting that k_1 is in the high-pressure limit for $P > 1.5$ atm and $T < 1200$ K.

A similar shock tube study was reported by Kern et al.[9] at temperatures from 1200 to 1800 K and pressures from 0.19 to 0.40 atm. They suggested that

$$k_1\,(s^{-1}) = (2.6 \times 10^{13})e^{-58.6(\text{kcal/mol})/RT}$$

with $k_{1a} = 0.54k_1$ and $k_{1b} = 0.46k_1$. At 1200 K, the total rate constant reported by Kern et al.[9] is about a factor of 5 smaller than that of Lifshitz et al.[8] The cause for the discrepancy is unclear, though the pressure falloff may contribute to this discrepancy. There have been several ignition delay studies[10−13] for ethylene oxide oxidation. The oxidation of ethylene oxide has also been studied in a jet-stirred reactor at temperatures between 800 and 1150 K and at pressures from 1 to 10 atm.[14]

Mechanistically, the unimolecular decomposition of ethylene oxide has been an interesting theoretical problem, as the reaction can proceed on both the singlet and triplet potential energy surfaces. Observations of the isomerization of triplet C_2H_4O biradicals isomers, including $^{\bullet}CH_2-O-CH_2^{\bullet}$, $^{\bullet}CH_2CH_2O^{\bullet}$, and $CH_3{}^{\bullet\bullet}CHO$ showed that $^{\bullet}CH_2-O-CH_2^{\bullet}$ isomerizes mainly to ethylene oxide, and not to methoxycarbene, while $^{\bullet}CH_2CH_2O^{\bullet}$ isomerizes mainly to acetaldehyde (CH_3CHO).[15] This observation led to the suggestion that ethylene oxide decomposition starts by C−O fission to form the triplet $^{\bullet}CH_2CH_2O^{\bullet}$, followed by 1,2-H shift to form CH_3CHO. A subsequent QCISD/6-31G(D) study[16] suggested, however, that the unimolecular decomposition of ethylene oxide starts from its isomerization to acetaldehyde on the singlet surface (see Scheme 1) with an activation energy $E_{1a} = 46$ kcal/mol. This is followed by the unimolecular decomposition of CH_3CHO, i.e.,

$$CH_3CHO \rightarrow CH_4 + CO$$

* Address correspondence to these authors. E-mail: T.A.B., tim.barckholtz@exxonmobil.com; H.W., haiw@usc.edu.
[†] University of Delaware.
[‡] University of Southern California.
[§] ExxonMobil Research and Engineering Company.

10.1021/jp0516442 CCC: $30.25
Published on Web 08/12/2005

SCHEME 1

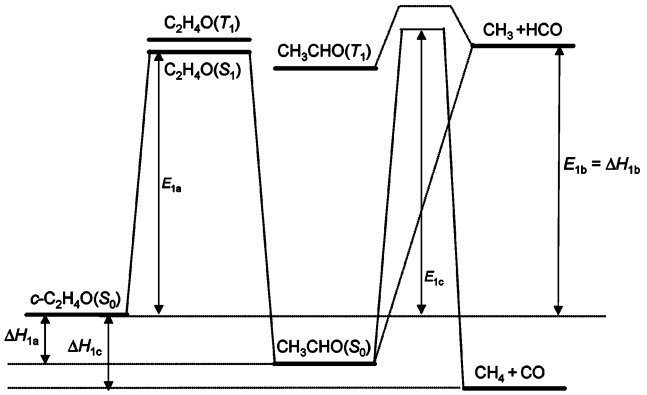

with an activation energy equal to 92 kcal/mol, or by spin state crossing to form triplet CH_3••CHO, which then dissociates to CH_3 + HCO, with an overall activation energy also equal to 92 kcal/mol for the overall reaction

$$CH_3CHO \rightarrow CH_3 + HCO$$

Here, we note that the initial isomerization energy barrier of $E_{1a} = 46$ kcal/mol is substantially lower than that measured experimentally.[8,9] Furthermore, the overall activation energy for reaction channels 1b and 1c would be $E_{1b} = E_{1c} = 63$ kcal/mol, or about 5 kcal/mol larger than observed activation energies (57−59 kcal/mol).

The unimolecular decomposition of acetaldehyde was also studied extensively. Yadav and Goddard[17] examined the isomerization of CH_3CHO to CH_3COH and CH_3OCH, and found the energy barriers to be ∼90 kcal/mol for CH_3COH and ∼100 kcal/mol for CH_3OCH. It follows that the CH_3COH channel could be viable for c-C_2H_4O decomposition, since $\Delta H_{1a} = 27$ kcal/mol, giving the overall activation energy of $E_a = \sim 90-27 \approx 63$ kcal/mol for c-$C_2H_4O \rightarrow CH_3COH$. A similar conclusion may be reached by examining the G1 results of Smith et al.[18] Yadav and Goddard[19] investigated the radical and molecular dissociation of CH_3CHO using SCF calculations and reported the C−C bond energy in CH_3CHO to be 76 kcal/mol, while molecular decomposition of CH_3CHO (2c) requires 84 kcal/mol activation energy, or 8 kcal/mol lower than that of the QCISD/6-31G(D) result.[16] Additional studies support the lower activation energy value, e.g., 83 kcal/mol by G2 and 81 kcal/mol at the B3LYP/cc-PVTZ(-f) level of theory.[20,21] Assuming that $E_{1a} = 46$ kcal/mol,[16] we may now estimate that $E_{1b} = 46$ to 49 kcal/mol and $E_{1c} = 57$ kcal/mol. While E_{1c} is in close agreement with the observed activation energy, the E_{1b} value is too small to explain the observed activation energies of channel 1b. Therefore, either the E_{1a} value reported in ref 16 is too small, or the activation energies reported for reaction $CH_3CHO \rightarrow CH_3 + HCO$ in refs 19−21 are all too small.

Despite these uncertainties, it is generally accepted that the isomerization of c-C_2H_4O to form CH_3CHO proceeds through C−O rupture to form the •CH_2CH_2O• biradical, followed by 1,2-H shift in the biradical to form CH_3CHO.[22−27] The singlet and triplet states of •CH_2CH_2O• are expected to be very close, with differences attributable almost entirely to the O−C−C−H dihedral angle, as illustrated in Figure 1. Because the two electrons that form the biradical are separated in space and with little electronic coupling, the spin pairing energy is small and the singlet and triplet states are close in energy. Furthermore, as explained in detail later, the biradical nature of •CH_2CH_2O• makes it not amenable to standard ab initio and DFT methods that rely on a single configuration reference wave function.

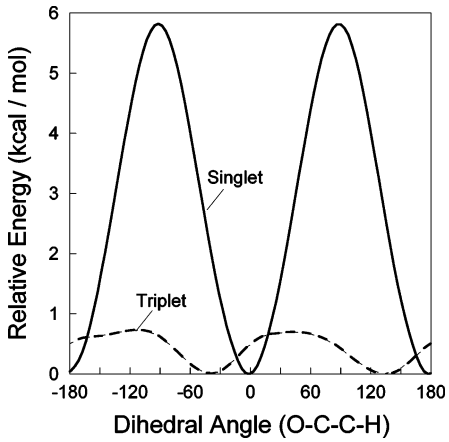

Figure 1. Energies of the open-shell singlet and triplet states of the •CH_2CH_2O• biradical relative to their respective minimal energies, as computed at the UB3LYP/6-31G(d) level.

Using SCF methods, Bigot et al.[22] calculated the energy barriers for C−O and C−C bond rupture in c-C_2H_4O. The C−O bond rupture on the singlet surface to form the •CH_2CH_2O• biradical was found to be energetically favored. The reverse ring-closure has little to no energy barrier. The biradical was found to exist in the degenerate singlet and triplet states, indicating the possibility of facile intersystem crossings. Using the spin-unrestricted Hartree−Fock (UHF) formalism, Yamaguchi and co-workers[23] concluded that among several singlet and triplet biradical isomers, the triplet state was more stable than the lowest singlet state, which lies 1.2 kcal/mol above the triplet. Using the DZP basis set, Dupuis et al.[24] refined the above calculations and concluded that a triplet state is the most stable structure for the biradical. Approximately projected UHF Møller−Plesset calculations of Fueno et al.[25] showed a singlet state to be the most stable of all the singlet and triplet states considered. Clearly, the relative stability of the lowest lying singlet and triplet biradical and the exact energy splitting are beyond the realm of theory at the level of computational complexity attempted. Nevertheless, the small energy splitting in the two states supports the notion of a facile intersystem crossing. Indeed Knuts et al.[27] calculated the spin−orbit coupling by multiconfigurational linear response theory and predicted a large probability for the crossing. While the singlet−triplet crossing is not relevant to the current work, it is a critical feature in the PES of the reaction of atomic oxygen with ethylene.

Previously, an energy barrier of 9 kcal/mol was reported for the 1,2-H shift to CH_3CHO in the biradical singlet manifold, giving a total activation energy of $E_{1a} = 64$ kcal/mol for the isomerization of ground state c-C_2H_4O to CH_3CHO.[24] It should be noted here that the observation of methyl and formyl radicals from the C_2H_4 + O reaction can be explained only by a 1,2-H shift in the •CH_2CH_2O• adduct on the singlet surface. Calculations to be reported in the present work show that a similar 1,2-H shift on the triplet surface has a much larger critical energy. Thus, chemistry on the triplet surface can be safely disregarded for the decomposition reactions of c-C_2H_4O.

The above discussion points to the facts that (a) a quantitative energy barrier for the isomerization of c-C_2H_4O to CH_3CHO is not available, (b) this isomerization is complicated by intersystem crossing, and (c) as a result the existing kinetic data for ethylene oxide unimolecular decomposition remain to be theoretically explained. The objective of the present work was to provide a more definite description for the mechanism and kinetics of ethylene oxide decomposition. To accomplish this objective, quantum chemistry calculations were carried out, and

the rate constants for ethylene oxide decomposition were examined by RRKM/Master Equation Solution analysis, for reaction channels that have and have not been considered before, including

$$c\text{-}C_2H_4O \rightarrow CH_3CHO \quad \text{(R1a)}$$
$$\rightarrow CH_3 + HCO \quad \text{(R1b)}$$
$$\rightarrow CH_4 + CO \quad \text{(R1c)}$$
$$\rightarrow CH_3CO + H \quad \text{(R1d)}$$
$$\rightarrow CH_2CHO + H \quad \text{(R1e)}$$
$$\rightarrow CH_2CO + H_2 \quad \text{(R1f)}$$
$$\rightarrow C_2H_2 + H_2O \quad \text{(R1g)}$$
$$\rightarrow C_2H_3OH \quad \text{(R1h)}$$

In addition, the unimolecular decomposition of oxiranyl radical (c-C_2H_3O) and the chemically activated reaction between c-C_2H_4O and H were studied similarly. Through G3 and RRKM/Master Equation analysis, we obtained rate constant estimates for

$$c\text{-}C_2H_3O \rightarrow CH_3 + CO \quad \text{(R2a)}$$
$$\rightarrow CH_2CO + H \quad \text{(R2b)}$$
$$\rightarrow CH_2CHO \quad \text{(R2c)}$$

$$c\text{-}C_2H_4O + H \rightarrow CH_3CHO + H \quad \text{(R4)}$$

Detailed kinetic modeling of ethylene oxide pyrolysis followed. We used an elementary reaction mechanism, consisting of 332 reactions and 45 species. It will be shown below that kinetic modeling reconciles the results of quantum chemistry calculations and reaction rate theory analysis with the single-pulse shock tube data of Lifshitz et al.[8]

Computational Methods

Quantum Chemical Calculations. All quantum chemical calculations were performed using Gaussian03.[28] The geometry of each species was first optimized using the hybrid B3LYP density functional theory, which employs a slightly modified Becke's three-parameter exchange functional (B3)[29,30] coupled with the correlation functional of Lee, Yang, and Parr (LYP).[31] The geometry optimization used the 6-31G(d) basis set. The B3LYP/6-31G(d) energies were further refined through a full G3B3 calculation,[32] except for the critical geometry of reaction 1a and the $^{\bullet}CH_2CH_2O^{\bullet}$ biradical, which requires further consideration, as will be discussed later. The critical geometries were determined with the combined synchronous transit and quasi-Newton method.[33] The critical geometries were confirmed by the presence of a single imaginary frequency and by intrinsic reaction coordinate calculations.[34] For radical−radical association reactions, the absence of a pronounced energy barrier was confirmed by a relaxed scan of the potential energy surface. To obtain more accurate molecular parameters for rate calculation, we optimized further the geometries of all the species using the 6-311++G(d,p) basis set. The harmonic frequencies obtained at this level were scaled by a factor of 0.99 to obtain the zero-point energies.

Because the $^{\bullet}CH_2CH_2O^{\bullet}$ biradical is an open-shell singlet, standard single-configuration methods cannot even qualitatively calculate its energy and the energy of its transition states. The ubiquitous Hartree−Fock calculation, and all of the methods that use a HF reference wave function, such as the Møllet−Plesset, QCISD(T), and other higher level calculations, are inappropriate for this biradical. The most suitable approach is to use a multiconfiguration wave function, such as the CASSCF method. However, there are problems with this approach, including the difficulty in converging these calculations and in achieving high accuracy with them. These problems were indeed encountered in the present study, as our CASSCF calculation often failed to consistently define the active space. For this reason and as a preliminary alternative to a good CASSCF calculation, we used *unrestricted singlet wave functions* to estimate the biradical character and the transition states that connect to it. Such wave functions have been shown to be not the true wave function of the open-shell singlet state, but for this biradical and its transition states (all of which are reasonably tight transition states), the unrestricted singlet wave function is a reasonable approximation.

It has been well established that the unrestricted singlet wave function is contaminated with the corresponding triplet wave function, and a simple procedure has been developed to obtain the open-shell singlet energy with the first-order contribution of the triplet state removed. This spin-projection procedure was used at each step in the G3 calculation; that is, each Møllet−Plesset or QCISD(T) calculation was performed for both the unrestricted singlet and triplet states, and the open-shell singlet energy computed using the approach of Yamaguchi et al.[35] The $\langle S^2 \rangle$ values, required for the spin-projection procedure, were found to be ~1.0 and 2.0 for these singlet and triplet calculations, respectively. We do not expect these calculations to be as accurate as the normal G3 approach for closed shell singlets, but we do expect them to be considerably more accurate than if a closed shell singlet wave function is used for the reference wave function in the G3 components. We are currently pursuing several alternatives for the refinement of these energies, including CASSCF calculations and the spin-flip method of Krylov and co-workers.[36]

Rate Constant Evaluation. The microcanonical rate constants were calculated with the conventional RRKM expression,[37,38]

$$k(E) = l_a \frac{Q^{\dagger}_{r,in}}{Q_{r,in}} \frac{W(E^{\dagger})}{h\rho(E)}$$

where l_a is the reaction path degeneracy, the ratio of partition functions Q accounts for adiabatic rotations (the subscript *r,in* denotes an external inactive rotor), $W(E^{\dagger})$ is the sum of states at energy level $E^{\dagger} = E - E_0$ for the active degrees of freedom in the activated complex, E_0 is the energy barrier, $\rho(E)$ is the density of states for the active degrees of freedom in the stable geometries, and h is the Planck constant. All active modes were treated by the rigid-rotor, harmonic-oscillator approximation. The density and sum of states were computed with the Whitten−Rabinovitch approximation.[39] Active free rotors were treated with the method of Astholz et al.[40] The thermal rate constants were computed with an in-house Monte Carlo code for the RRKM/Master Equation analysis. Details are discussed elsewhere.[41]

Detailed Kinetic Modeling. Simulation of the single-pulse shock tube experiments of ethylene oxide decomposition was carried out, using the ChemKin Suite of program,[42] under the isobaric condition. The reaction mechanism, consisting of 332 reactions and 45 species, was derived from earlier studies.[43−47] Specifically, the H_2/CO pyrolysis model was taken from Davis

TABLE 1: Selected Key Reactions for the Thermal Decomposition of Ethylene Oxide

		rate parameters[a]			
no.	reaction	*A*	*n*	*E*	ref/comments
1a	*c*-$C_2H_4O \leftrightarrow CH_3CHO$	3.18×10^{12}	−0.76	46424	p.w.[c]
1b	*c*-$C_2H_4O \leftrightarrow CH_3 + HCO$	5.57×10^{13}	0.40	61884	p.w.[b]
1c	*c*-$C_2H_4O \leftrightarrow CH_4 + CO$	1.07×10^{13}	0.11	63783	p.w.[c]
1d	*c*-$C_2H_4O \leftrightarrow CH_3CO + H$	2.43×10^{13}	0.25	65310	p.w.[c]
1e	*c*-$C_2H_4O \leftrightarrow CH_2CHO + H$	1.84×10^{13}	0.20	71781	p.w.[c]
1f	*c*-$C_2H_4O \leftrightarrow CH_2CO + H_2$	3.57×10^{12}	−0.20	63033	p.w.[c]
1g	*c*-$C_2H_4O \leftrightarrow C_2H_2 + H_2O$	7.63×10^{12}	0.06	69531	p.w.[c]
2a	*c*-$C_2H_3O \leftrightarrow CH_3 + CO$	7.31×10^{12}		14280	p.w.[c]
2b	*c*-$C_2H_3O \leftrightarrow CH_2CO + H$	4.96×10^{13}		14863	p.w.[c]
2c	*c*-$C_2H_3O \leftrightarrow CH_2CHO$	8.74×10^{31}	−6.90	14994	p.w.[c]
3	$CH_2CO + H \leftrightarrow CH_3 + CO$	1.97×10^{7}	1.927	1755	p.w.
4	*c*-$C_2H_4O + H \leftrightarrow CH_3CHO + H$	5.00×10^{13}		9000	p.w., est.
5	*c*-$C_2H_4O + H \leftrightarrow$ *c*-$C_2H_3O + H_2$	2.00×10^{13}		8300	8
6	*c*-$C_2H_4O + H \leftrightarrow C_2H_4 + OH$	9.51×10^{10}		5000	8
7	*c*-$C_2H_4O + O \leftrightarrow$ *c*-$C_2H_3O + OH$	1.91×10^{12}		5250	48
8	*c*-$C_2H_4O + OH \leftrightarrow$ *c*-$C_2H_3O + H_2O$	1.78×10^{13}		3610	49
9	*c*-$C_2H_4O + CH_3 \leftrightarrow$ *c*-$C_2H_3O + CH_4$	1.07×10^{12}		11830	49

[a] Units: cm^3, s, cal, and mol, [b] p.w. = present work, [c] Computed for an Ar pressure of 2 atm and temperatures ranging from 300 to 2000 K.

et al.[43] and most of the C_1-C_2 chemistry from the GRI-Mech (version 1.2).[44] The C_3 hydrocarbon chemistry was taken from refs 45−47. With a few exceptions, most of these reactions do not exhibit strong sensitivity for the shock-tube experiment of ethylene oxide decomposition, as will be discussed later.

Reactions relevant to ethylene oxide decomposition were then added to the reaction mechanism. Their rate constants were either calculated in the present work or taken from the literature. Key reactions and their rate parameters are presented in Table 1.

Results

Table 2 lists the enthalpies of formation of some of the major species taken from the literature. The relative energies of the species computed at the G3B3 level were compared with these literature values (Table 3). As can be seen, the agreement is within ±1 kcal/mol for all species considered.

Unimolecular Decomposition of Ethylene Oxide. Details of the potential energy surface of the ethylene oxide decomposition are presented in Figure 2. As discussed before, the first step in the decomposition of *c*-C_2H_4O (**1**) is the ring-opening via C−O bond rupture, leading to a biradical intermediate, $^{\bullet}CH_2CH_2O^{\bullet}$ (**2**). An H-atom 1,2-shift from this biradical (**2**) leads to acetaldehyde (**3**). A similar 1,2-H shift to form vinyl alcohol (**4**) is possible though our extensive search on the PES failed to locate an appropriate transition state for this isomerization. As expected, the closed shell singlet G3 calculation predicted the singlet, open-ring $C_2H_4O(S_1)$ (**2**) to be 88 kcal/mol, over 28 kcal/mol too high compared to the observed activation energy. Furthermore, the G3 energy barrier for the ring opening and 1−2 H-shift (66 and 75 kcal/mol, respectively) are substantially smaller than the energy of the intermediate $C_2H_4O(S_1)$ for these transitions, indicating the inadequacy of single-referenced wave functions as discussed previously.

Single-point calculations for the unrestricted, singlet energies (USE) yielded lower critical energy, and ranged from 54 to 68 kcal/mol for *c*-$C_2H_4O(S_0)$ (**1**) → $C_2H_4O(S_1)$ (**2**) at several levels of theory as shown in Table 4. In general, the spin correction procedure described earlier led to a further decrease in the critical energy, by ∼1 kcal/mol, as seen in Table 4 (SCE). Several observations may be made from the energy values resulting from this spin correction procedure. First, although notable discrepancies are seen among different levels of theory, these critical energies are generally smaller than the closed shell singlet G3 values. The variation of the critical energies has little to no correlation with the basis set size. Second, the MP4, spin-corrected singlet energy for **1** → **2** is in line with the observed activation energy of 57−59 kcal/mol,[8,9] thereby giving the justification that reaction 1a may be modeled with a critical energy around 60 kcal/mol. Third, the critical energies of C−O rupture and 1,2-H atom shift are roughly equal, and $C_2H_4O(S_1)$ (**2**) represents a shallow well atop the energy barrier of *c*-$C_2H_4O(S_0)$ (**1**) isomerization to CH_3CHO (**3**). Hence, the isomerization will be treated as a single-step process. Last, the total unimo-

TABLE 2: Enthalpies of Formation (kcal/mol) of Key Species Used in This Study

species	$\Delta H_{f,298K}$	ref	species	$\Delta H_{f,298K}$	ref
c-C_2H_4O	−12.6	*a*	CH_3	35.1	*i*
CH_3CHO	−39.7	*b*	HCO	10.0	*i*
C_2H_3OH	−29.8	*c*	H_2O	−57.8	*a*
CH_2CHO	3.1	*d*	CO	−26.4	*a*
CH_3CO	−2.5	*e*	H	52.1	*j*
CH_2CO	−11.9	*f*	C_3H_8	−25.0	*k*
C_2H_2	54.5	*g*	*c*-C_3H_5	69.3	*l*
H_2CC	99.1	*h*	CH_3OCH_3	−44.0	*b*
CH_4	−17.8	*a*	*c*-C_2H_3O	39.6	*m*

[a] Chase, M. W., Jr. *NIST-JANAF Themochemical Tables*, 4th ed.; J. Phys. Chem. Ref. Data, Monogr. 9; American Chemical Society: Washington, DC, 1998; p 1. [b] Chao, J.; Hall K. R.; Marsh, K. N.; Wilhoit, R. C. *J. Phys. Chem. Ref. Data* **1986**, *15*, 1369. [c] Holmes, J. L.; Lossing, F. P. *J. Am. Chem. Soc.* **1982**, *104*, 2648. [d] Bouchoux G.; Chamot-Rooke, J; Leblanc, D.; Mourgues, P.; Sablier M. *ChemPhysChem* **2001**, *4*, 235. [e] Niiranen J. T.; Gutman, D.; Krasnoperov, L. N. *J. Phys. Chem.* **1992**, *96*, 5881. [f] Ruscic, B.; Litorja, M.; Asher, R. L. *J. Phys. Chem. A* **1999**, *103*, 8625. [g] Pedley, J. B.; Naylor, R. D.; Kirby, S. R. *Thermochemical Data of Organic Compounds;* Chapman and Hall: London and New York, 1986. [h] Chen, Y. Q.; Jonas, D. M.; Kinsey, J. L.; Field, R. W. *J. Chem. Phys.* **1989**, *91*, 3976. [i] Tsang, W., Heats of Formation of Organic Free Radicals by Kinetic Methods. In *Energetics of Organic Free Radicals*; Martinho Simoes, J. A., Greenberg, A., Liebman, J. F., Eds.; Blackie Academic and Professional: London, UK, 1996; p 22. [j] *JANAF Thermochemical Tables;* Natl. Stand. Ref. Data Ser.; U.S. National Bureau of Standards: Washington, DC, 1985; Vol. 37. [k] Pittam, D. A.; Pilcher, G. *J. Chem. Soc., Faraday Trans. 1* **1972**, *68*, 2224. [l] Burcat, A.; Ruscic, B. *Third Millennium Ideal Gas and Condensed Phase Thermochemical Database for Combustion with updates from Active Thermochemical Tables*; Technion-IIT, Aerospace Engineering: Haifa, Israel; Argonne National Laboratory, Chemistry Division: Argonne, Illinois, 2005. [m] This work, using isodesmic reactions (see text for details).

TABLE 3: Comparison of G3B3 Energies Relative to Ground State Acetaldehyde with Available Thermochemical Data

species	E (hartree)	ΔE_{0K} (kcal/mol)	ΔE_{298K} (kcal/mol)	$\Delta E_{298,lit}$[a] (kcal/mol)	difference (kcal/mol)
c-C_2H_4O	−153.674115	27.7	27.3	27.1	0.2
C_2H_3OH	−153.700397	10.3	10.2	10.0	0.2
$CH_2CHO + H$	−153.568516	93.9	94.7	94.9	−0.2
$CH_3CO + H$	−153.578060	87.9	88.8	89.4	−0.6
$CH_3 + HCO$	−153.587714	81.9	83.8	84.8	−1.0
$C_2H_2 + H_2O$	−153.662428	35.0	36.8	36.5	0.3
$H_2CC + H_2O$	−153.592857	78.6	80.7	81.1	−0.4
$CH_2CO + H_2$	−153.677733	25.4	27.3	27.9	−0.6
$CH_4 + CO$	−153.728249	−6.3	−4.8	−4.5	−0.3

[a] Based on the literature data (see Table 1).

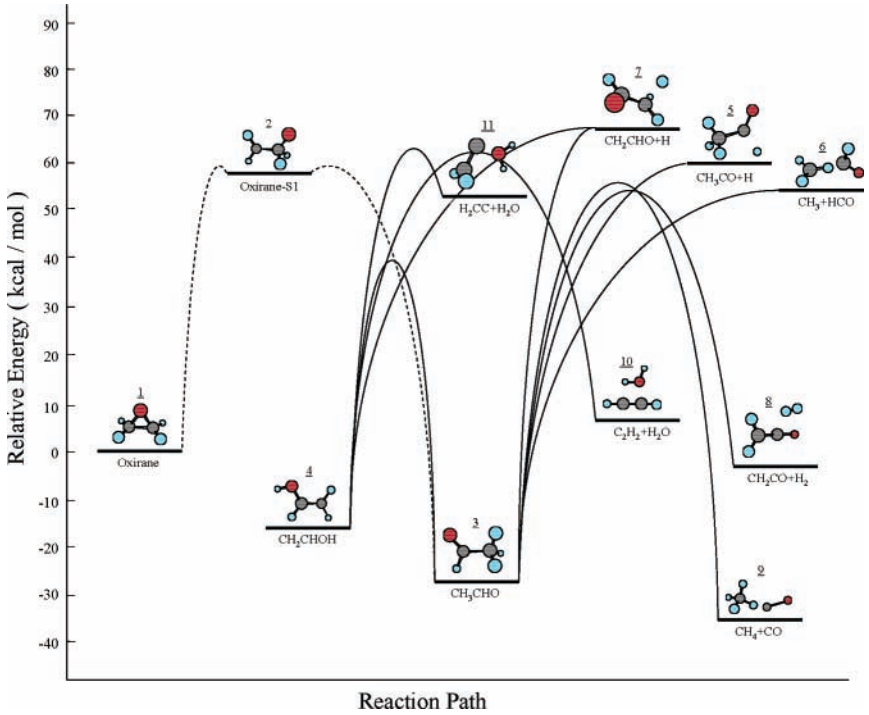

Figure 2. Potential energy barriers of the ethylene oxide system, determined at the G3B3 level of theory. The dashed line represents an approximation for the initial isomerization step (see text and Table 4 for details).

lecular rate constant is expected to be the most sensitive to the isomerization energy barrier, as the subsequent decomposition channels of acetaldehyde to form $CH_3 + HCO$ (**6**) and $CH_4 + CO$ (**9**) barriers are lower in energy than the isomerization barrier. Unfortunately, it is the isomerization energy barrier that has the highest uncertainty. We are therefore forced to treat this critical energy as an adjustable parameter in the RRKM analysis by fitting the shock tube data of Lifshitz et al.[8]

At the G3B3 level of theory we calculated the energy barrier for the isomerization of triplet ethylene oxide to triplet acetaldehyde to be 91 kcal/mol above c-$C_2H_4O(S_0)$. The possibility of unimolecular decomposition of $C_2H_4O(S_1)$ that occurs on the triplet surface may be safely disregarded. The rest of the potential energy surface was calculated at the G3B3 level and shown in Figure 2 by solid lines. The excited acetaldehyde formed upon thermal activation of ethylene oxide can undergo several competing isomerization and decomposition steps. Formation of CH_3 and HCO radicals upon rupture of the C−C bond is energetically the most favorable. The energy required for this process was calculated to be 81.9 kcal/mol above the ground-state acetaldehyde. Other dissociation channels include the H-elimination from acetaldehyde. The molecular decomposition pathways of acetaldehyde include the CO- and H_2-elimination. The critical energies and heats of reaction of these pathways compare well with the earlier studies,[18−21] as seen in Table 5.

Acetaldehyde can also undergo unimolecular rearrangement to form vinyl alcohol (C_2H_3OH, **4**) and hydroxyethylidene (CH_3-COH). The current calculations predict C_2H_3OH to lie 11.2 kcal/mol above acetaldehyde (**3**), in excellent agreement with the previously calculated value.[18] The critical geometry of **3** → **4** was calculated to lie 67.5 kcal/mol above acetaldehyde, in good agreement with the previously reported value of 67.4 kcal/mol.[17] Vinyl alcohol can lose H_2O via two competing pathways, one that leads to the formation of acetylene (**10**), and the other to vinylidene (**11**). While the unimolecular decomposition to vinylidene is more endothermic as compared to that producing acetylene, the facile insertion of vinylidene in the O−H bond of water leads to a much smaller activation energy for its reverse reaction.

The fragmentation of vinyl alcohol (**4**) to form the vinyl radical is highly endothermic (106 kcal/mol) and hence this channel was excluded in our rate calculations. The formation of hydroxyethylidene from acetaldehyde was calculated to be endothermic by 50.9 kcal/mol, again in excellent agreement with the previously calculated value.[18] The critical energies required for the isomerization of acetaldehyde and vinyl alcohol to

TABLE 4: Absolute and Relative Single-Point Energies of Singlet Biradicals at Various Levels of Theory, Using the Spin Correction Procedure (See Text).

	c-$C_2H_4O(S_0)$	$^{\bullet}CH_2CH_2O^{\bullet}(C_2H_4O\text{-}S_1)$					
method	singlet (hartree)	restricted (hartree)	RSE[b] (kcal/mol)	singlet (hartree)	triplet (hartree)	USE[c] (kcal/mol)	SCE[d] (kcal/mol)
MP2//6-31G(d)	−153.30348	−153.16276	83.27	−153.19254	−153.19133	64.58	63.82
MP2//6-31+G(d)	−153.31453	−153.18411	76.80	−153.20390	−153.20255	64.38	63.54
MP2//6-31+G(2df,p)	−153.42341	−153.27996	84.98	−153.30683	−153.30533	68.11	67.17
MP4//6-31G(d)	−153.34140	−153.22770	66.31	−153.24054	−153.23886	58.26	57.20
MP4//6-31+G(d)	−153.35322	−153.24461	63.12	−153.25288	−153.25101	57.93	56.75
MP4//6-31+G(2df,p)	−153.46938	−153.35057	69.52	−153.36290	−153.36095	61.78	60.55
QCISD(T)//6-31G(d)	−153.34138	−153.19249	88.40	−153.24664	−153.24286	54.41	52.04
G3	−153.67411		88.66	−153.53282			

	TS for $S_0 \rightarrow S_1$					
method	restricted (hartree)	RSE[b] (kcal/mol)	singlet (hartree)	triplet (hartree)	USE[c] (kcal/mol)	SCE[d] (kcal/mol)
MP2//6-31G(d)	−153.16647	81.70	−153.19207	−153.18833	65.64	63.29
MP2//6-31+G(d)	−153.18520	76.89	−153.19911	−153.19972	68.16	68.54
MP2//6-31+G(2df,p)	−153.28200	84.46	−153.30145	−153.30212	72.26	72.68
MP4//6-31G(d)	−153.22859	66.52	−153.24002	−153.23594	59.35	56.80
MP4//6-31+G(d)	−153.24585	63.11	−153.24796	−153.24832	61.78	62.01
MP4//6-31+G(2df,p)	−153.35146	69.72	−153.35753	−153.35794	65.92	66.17
QCISD(T)//6-31G(d)	−153.22982	65.74	−153.24457	−153.23981	56.48	53.50
G3		66.44	−153.56824			

	TS for $S_1 \rightarrow CH_3CHO$					
method	restricted (hartree)	RSE[b] (kcal/mol)	singlet (hartree)	triplet (hartree)	USE[c] (kcal/mol)	SCE[d] (kcal/mol)
MP2//6-31G(d)	−153.18457	69.49	−153.18351	−153.17627	70.15	65.61
MP2//6-31+G(d)	−153.20416	64.12	−153.19533	−153.18754	69.66	64.77
MP2//6-31+G(2df,p)	−153.30389	69.87	−153.29983	−153.29204	72.41	67.52
MP4//6-31G(d)	−153.24291	56.68	−153.23173	−153.22366	63.69	58.63
MP4//6-31+G(d)	−153.26084	52.83	−153.24457	−153.23585	63.05	57.57
MP4//6-31+G(2df,p)	−153.33686	78.03	−153.35603	−153.34738	66.00	60.57
QCISD(T)//6-31G(d)	−153.23608	60.95	−153.24208	−153.22801	57.18	48.36
G3			−153.55452		75.05	

[a] The geometries are optimized at the B3LYP/6-31G(d) level of theory, using an unrestricted wavefunction for the biradical intermediate and its transition states. [b] RSE = restricted singlet energy without spin correction relative to the energy of *c*-$C_2H_4O(S_0)$, including zero-point energy correction. [c] USE = unrestricted singlet energy without spin correction relative to the energy of *c*-$C_2H_4O(S_0)$, including zero-point energy correction. [d] SCE = spin-corrected singlet energy relative to the energy of *c*-$C_2H_4O(S_0)$, including zero-point energy correction.

TABLE 5: Comparison of Critical Energies (E_a, kcal/mol) and Heats of Reaction (ΔH_{0K}, kcal/mol) for the Molecular Decomposition Channels

reaction	ref 18	ref 19	ref 20	ref 21	this work
$CH_3CHO \rightarrow CH_4 + CO$					
E_a	82.9	84.4	82.9	81.1	83.0
ΔH_{0K}	−6.9	−13.5	− 5.9[a]	−1.7[b]	−6.3
$CH_3CHO \rightarrow CH_2CO + H_2$					
E_a	81.0		81.3		81.0
ΔH_{0K}	25.6		27.7[a]		25.4

[a] Reaction enthalpy obtained at 298 K. [b] Does not include zero-point energies.

hydroxyethylidene were calculated as 66.2 and 62.7 kcal/mol, respectively. While the latter is in good agreement with the calculated value of Smith et al. (63.1 kcal/mol),[18] the former is much lower than their value of 79.1 kcal/mol. Indeed, the authors noted that the energy ordering of the transition states for the rearrangements of hydroxyethylidene to vinyl alcohol and acetaldehyde as obtained from their theoretical study was inconsistent with the experimental observation.[49] The current study supports the experimental observation that hydroxyethylidene should require lesser energy to isomerize to acetaldehyde, as compared to vinyl alcohol. For the present study, however, hydroxyethylidene is unimportant. Its fragmentation to form methane requires a further 55 kcal/mol.[18] The shallow energy well also precludes significant collision stabilization. We chose not to include this species in the rate calculations.

Thermal rate constants were calculated for the unimolecular decomposition of ethylene oxide, using the RRKM parameters presented in Table 6. The transition state parameters for the isomerization of ethylene oxide to acetaldehyde were taken from that connecting ring-opened $C_2H_4O(S_1)$ and acetaldehyde. The loose transition states associated with the dissociation of CH_3-CHO (**3**) were treated by assigning appropriate rate constant values at the high-pressure limit for the reverse radical−radical association reactions: $k_\infty(CH_2CHO+H) = k_\infty(CH_3CO+H) = 10^{14}$ cm^3 mol^{-1} s^{-1} and $k_\infty(CH_3+HCO) = 2 \times 10^{13}$ cm^3 mol^{-1} s^{-1}. The rotational constants of the external, inactive rotors in these transition states were adjusted to fit these k_∞ values.

Figure 3 shows the total rate constant computed at 2 atm of pressure, using a nominal $E_{1a} = 59$ kcal/mol as the critical energy for the isomerization of *c*-C_2H_4 to CH_3CHO, with M = Ar and $\langle E_{down} \rangle = 260$ cm^{-1}. The number of stochastic trials was 250 000, whereas the total rate constant was fully converged using as little as 1000 such trials. The choice for the critical energy value will be discussed later. At this pressure, the total rate constant is almost at the high-pressure limit, which may be parametrized by

$$k_{1,\infty}(1/s) = (3.74 \times 10^{10}) T^{1.298} e^{-29990/T} \qquad (600 < T < 2000 \text{ K}).$$

A comparison with the observed rate constants of Lifshitz et al.[8] shows close agreement for $T > 1000$ K, but the computed

TABLE 6: RRKM Parameters of Ethylene Oxide Decomposition, Calculated at the B3LYP/6-311++G(d,p) Level of Theory (all frequencies scaled by 0.989)

c-C_2H_4O (**1**)	υ, cm^{-1}	808, 831, 876, 1028, 1128, 1137, 1152, 1159, 1286, 1486, 1520, 3049, 3056, 3130, 3145
	B_0,[a] cm^{-1}	0.79 (1,2) external inactive; 0.47 (2,1) external active
CH_3CHO (**3**)	υ, cm^{-1}	151,[b] 505, 767, 877, 1116, 1121, 1362, 1404, 1444, 1453, 1788, 2840, 2988, 3042, 3102
	B_0,[a] cm^{-1}	0.32 (1,2) external inactive; 1.91 (1,1) external active
C_2H_3OH (**4**)	υ, cm^{-1}	448, 485, 700, 816, 946, 980, 1106, 1300, 1334, 1429, 1674, 3106, 3157, 3204, 3768
	B_0,[a] cm^{-1}	0.32 (1,2) external inactive; 2.02 (1,1) external active
TS-1−3[c]	υ, cm^{-1}	237*i*, 410, 444, 695, 777, 930, 1048, 1156, 1240, 1292, 1434, 2622, 2813, 3099, 321
	B_0,[a] cm^{-1}	0.32 (1,2) external inactive; 1.75 (1,1) external active
	path degeneracy	2 for both forward and back reaction
TS-3−4	υ, cm^{-1}	2157*i*, 556, 632, 781, 954, 1051, 1123, 1181, 1279, 1444, 1518, 1839, 3051, 3076, 313
	B_0,[a] cm^{-1}	0.37 (1,2) external inactive; 1.62 (1,1) external active
	path degeneracy	1 for both forward and back reaction
TS-3−5[d]	υ, cm^{-1}	108,[b] 464, 844, 945, 1037, 1342, 1437, 1441, 1905, 2983, 3074, 3080
	B_0,[a] cm^{-1}	fitted to $k_\infty = 1 \times 10^{14}$ cm^3/mol·s for H + CH_3CO association (1,2) external inactive; 2.83 (1,1) external active; 0.32 (1,2) internal active (from CH_3CO)
TS-3−6[d]	υ, cm^{-1}	1088, 1913, 2625, 531, 1387, 1387, 3069, 3247, 3247
	B_0,[a] cm^{-1}	fitted to $k_\infty = 2 \times 10^{13}$ cm^3/mol·s for CH_3 + HCO association (1,2) external inactive; 9.54 (1,2) external active; 4.77 (6,1) internal active (from CH_3); 1.44 (1,2) internal active; 23.24 (1,1) internal active (from HCO);
TS-3−7[d]	υ, cm^{-1}	437, 502, 751, 963, 968, 1146, 1378, 1455, 1525, 2915, 3104, 3217
	B_0,[a] cm^{-1}	fitted to $k_\infty = 1 \times 10^{14}$ cm^3/mol·s for H + CH_2CHO association (1,2) external inactive; 2.24 (1,1) external active; 0.35 (1,2) internal active (from CH_2CHO)
TS-3−8	υ, cm^{-1}	1517*i*, 412, 557, 682, 849, 958, 1082, 1182, 1256, 1464, 1557, 1824, 2052, 3103, 3213
	B_0,[a] cm^{-1}	0.32 (1,2) external inactive; 2.14 (1,1) external active
	path degeneracy	1
TS-3−9	υ, cm^{-1}	1710*i*, 132,[b] 270, 520, 524, 748, 934, 1066, 1408, 1410, 1854, 2983, 3094, 3123, 3140
	B_0,[a] cm^{-1}	0.25 (1,2) external inactive; 1.62 (1,1) external active
	path degeneracy	1
TS-4−10	υ, cm^{-1}	1424*i*, 405, 533, 675, 742, 842, 862, 965, 1134, 1348, 1616, 1875, 3173, 3227, 3677
	B_0,[a] cm^{-1}	0.33 (1,2) external inactive; 1.49 (1,1) external active
	path degeneracy	1
TS-4−11	υ, cm^{-1}	1375*i*, 275, 301, 490, 595, 761, 864, 918, 1216, 1309, 1621, 2205, 3088, 3175, 3742
	B_0,[a] cm^{-1}	0.25 (1,2) external inactive; 1.74 (1,1) external active
	path degeneracy	1

[a] The numbers in parentheses are the symmetry number and the dimension of that rotor, in that order. [b] The torsional mode was treated as a free rotor. [c] TS-*i*−*j* represents transition state connecting species *i* and species *j*, with species numbers labeled in Figure 2. [d] The reaction path degeneracy of these reactions is folded into the rotational constant of the 2-dimension external rotor.

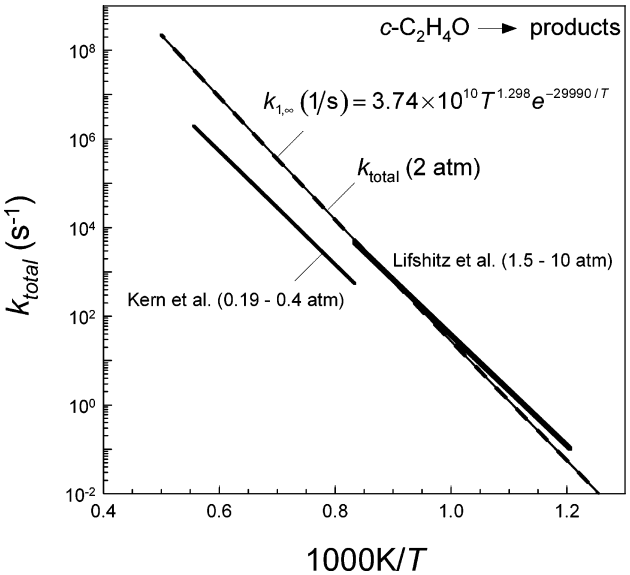

Figure 3. Total rate coefficient for unimolecular decomposition of ethylene oxide in argon. Computations used $E_{1a} = 59$ kcal/mol and $\langle E_{down} \rangle = 260$ cm^{-1}. The total rate coefficient computed at 2 atm is indistinguishable from the high-pressure limit rate coefficient.

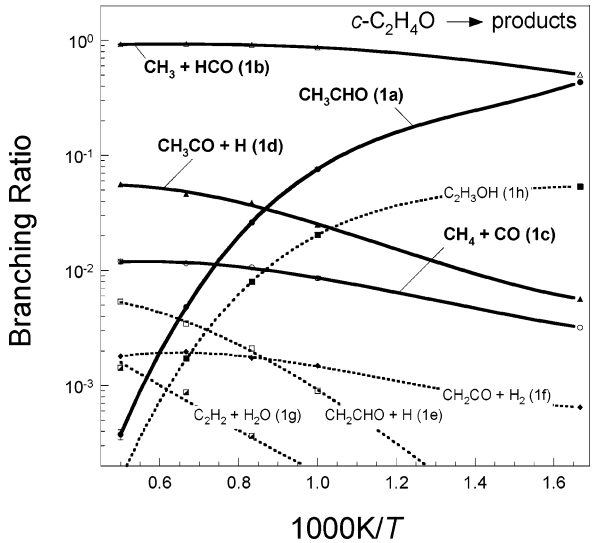

Figure 4. Branching ratio computed for unimolecular decomposition of ethylene oxide in argon at 2 atm. Computations used $E_{1a} = 59$ kcal/mol and $\langle E_{down} \rangle = 260$ cm^{-1}. Error bars represent one standard deviation and are mostly smaller than the symbols.

values are lower than the experimental counterpart by a factor of 2 at 800 K. A similar comparison with the rate constant reported by Kern et al. at lower pressure (0.19−0.4 atm) shows that the rate constant computed for reaction 1 at 0.2 atm is higher than their reported value by a factor of ~3 over the range of experimental conditions (1200−1800 K).

Figure 4 presents the branching ratios of reaction 1, computed at an argon pressure of 2 atm. Standard deviations from the stochastic simulations are shown for selected channels. It is seen that channel 1b is dominant over the entire temperature range. The CH_4 + CO channel 1c is seen to be the dominant molecular channel. The rate of the isomerization 1a is comparable with that of channel 1b at ~600 K, but it drops off considerably

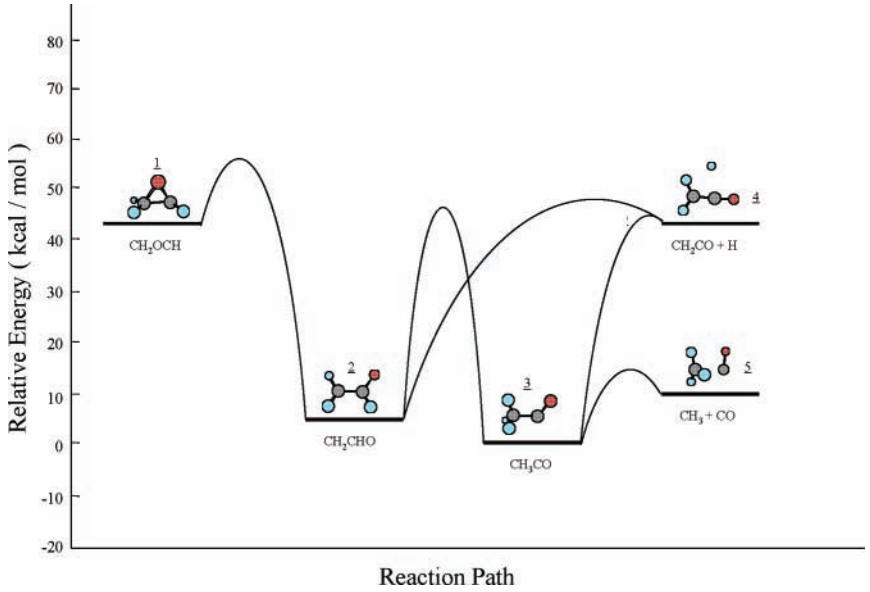

Figure 5. Potential energy barriers of the decomposition pathways of the oxiranyl radical, determined at the G3B3 level of theory.

above 1000 K. Channel 1g represents a sum of two separate channels leading to acetylene and vinylidene. While the rate constant for the formation of acetylene is seen to be the smallest, we found that the inclusion of channel 1g is critical to reproducing the acetylene concentrations in the thermal decomposition of ethylene oxide, especially toward ~1000 K. On the other hand, the result that k_{1g} is negligible below 1000 K is in accordance with the experimental observation as acetylene was not detected below 950 K.[8]

Unimolecular Decomposition of Oxiranyl Radical. Here we present our study of the unimolecular decomposition of the oxiranyl radical, an important intermediate formed upon H-abstraction of ethylene oxide. Figure 5 shows the potential energy surface calculated at the G3B3 level. The thermal decomposition of oxiranyl (**1**) is initiated by C−O β-scission. This step proceeds via a concerted rotation of the CH_2 group about the C−C bond to form the vinoxy radical (CH_2CHO, **2**), and it requires an activation energy of 13.5 kcal/mol. Vinoxy can further isomerize to the acetyl radical (CH_3CO, **3**) or it can lose an H atom to form ketene (**4**). The acetyl radical can also form ketene upon H elimination, or it can fragment to CH_3 and CO (**5**). In their study of the ketene + H reaction, Lee et al.[51] examined a part of this potential energy surface. The energies of stable intermediates and critical geometries of the present study compare well with that work. Thus, for instance, the activation energy of the H + ketene reaction to form the acetyl radical was calculated here to be 2.8 kcal/mol, compared to 2.5 kcal/mol with the CBS-APNO method.[51]

Table 7 shows the comparison of the relative energies of the species computed at the G3B3 level with those obtained using the literature thermochemical values (Table 1). The enthalpy of formation for *c*-C_2H_3O is highly uncertain. This led us to reexamine its thermochemistry. The following isodesmic reactions were chosen for this estimation:

$$c\text{-}C_2H_4O + CH_3 \leftrightarrow c\text{-}C_2H_3O + CH_4$$

$$c\text{-}C_2H_4O + C_2H_3 \leftrightarrow c\text{-}C_2H_3O + C_2H_4$$

$$c\text{-}C_2H_3O + C_3H_8 \leftrightarrow c\text{-}C_3H_5 + CH_3OCH_3$$

An average of the G3B3 and CBS-APNO calculations gives $\Delta H_{f,298} = 39.6$ kcal/mol for the oxiranyl radical. Using this value as the "literature" data (see Table 1), the G3B3 energy difference between the oxiranyl radical and the ground-state acetyl radical is 42.1 kcal/mol, in exact agreement with the "literature" data, as shown in Table 7.

TABLE 7: Comparison of G3 Energies (kcal/mol) Relative to the Ground-State Acetyl Radical with Literature Data

name of species	ΔE_{0K}	ΔE_{298K}	$\Delta E_{298,lit}$[a]
c-C_2H_3O	42.5	42.1	42.1[b]
CH_2CHO	6.0	5.9	5.6
$CH_2CO + H$	41.2	41.9	42.7
$CH_3 + CO$	8.4	10.0	11.1

[a] Based on the literature data (see Table 1). [b] Value determined from this work using the isodesmic reaction (see text).

Rate calculations were calculated for the unimolecular decomposition of oxiranyl using the methodology described earlier and with the RRKM parameters listed in Table 8. The rate coefficients for the various channels are plotted as a function of temperature in Figure 6. Again, the total rate constant was full converge with 1000 stochastic trials and the results shown in the figure represent calculations with 100000 trials. In Figure 6, the error bars are shown for selected temperatures, and they represent values of one standard deviation resulting from these trials.

It is seen that the oxiranyl radical primarily dissociates into ketene and H atom (2b). We also computed the rate coefficient for the ketene + H reaction,

$$CH_2CO + H \rightarrow CH_3 + CO \qquad \text{(R3)}$$

which occurs on the same potential energy surface, and compared our values with previous studies.[51,52−56] As can be seen in Figure 7, the calculated rate coefficient for the production of CH_3 and CO compares well with experimental data.[52−56] The present calculation yielded

$$k_3\,(\mathrm{cm^3/mol{\cdot}s}) = (1.97 \times 10^7)T^{1.927}e^{-883/T} \qquad \text{for } 300 \le T \le 2000\ \mathrm{K}$$

with little to no pressure dependency around the ambient pressure.

Simulation of the single pulse shock tube experiments[8] of ethylene oxide decomposition was carried out on the basis of

TABLE 8: RRKM Parameters for Oxiranyl Decomposition, Calculated at the B3LYP/6-311++G(d,p) Level with All Frequencies Scaled by 0.989 (see text)

c-C_2H_3O (**1**)	υ, cm^{-1}	761, 786, 927, 1026, 1056, 1112, 1164, 1338, 1504, 3060, 3100, 3152
	B_0,[a] cm^{-1}	0.63 (1,2) external inactive; 0.99 (2,1) external active
CH_2CHO (**2**)	υ, cm^{-1}	437, 502, 751, 963, 968, 1146, 1378, 1455, 1525, 2915, 3104, 3217
	B_0,[a] cm^{-1}	0.35 (1,2) external inactive; 2.23 (1,1) external active
CH_3CO (**3**)	υ, cm^{-1}	108,[b] 464, 844, 945, 1037, 1342, 1437, 1441, 1905, 2983, 3074, 3080
	B_0,[a] cm^{-1}	0.32 (1,2) external inactive; 2.83 (1,1) external active
TS-1−2[c]	υ, cm^{-1}	1114*i*, 554, 823, 874, 1026, 1078, 1293, 1333, 1474, 3060, 3129, 3160
	B_0,[a] cm^{-1}	0.51 (1,2) external inactive; 1.17 (1,1) external active
	path degeneracy	1 for both forward and back reaction
TS-2−3	υ, cm^{-1}	1525*i*, 432, 626, 842, 1020, 1109, 1198, 1432, 1810, 1878, 3007, 3196
	B_0,[a] cm^{-1}	0.33 (1, 2) external inactive; 3.39 (1,1) external active
	Path degeneracy	1 for forward reaction and 2 for back reaction
TS-2−4	υ, cm^{-1}	779*i*, 312, 481, 516, 586, 628, 984, 1131, 1390, 2116, 3128, 3243
	B_0,[a] cm^{-1}	0.32 (1,2) external inactive; 2.93 (1,1) external active
	path degeneracy	1
TS-3−4	υ, cm^{-1}	324*i*, 249, 409, 459, 552, 698, 987, 1138, 1383, 2188, 3139, 3232
	B_0,[a] cm^{-1}	0.30 (1,2) external inactive; 3.00 (1,1) external active
	path degeneracy	1
TS-3−5	υ, cm^{-1}	−272*i*, 36,[b] 237, 457, 496, 806, 1392, 1399, 2067, 3060, 3224, 3237
	B_0,[a] cm^{-1}	0.22 (1,2) external inactive; 1.95 (1,1) external active
	path degeneracy	1

[a] The numbers in parentheses are the symmetry number and the dimension of that rotor, in that order. [b] The torsional mode was treated as a free rotor. [c] TS-*i*−*j* represents transition state connecting species *i* and species *j*, with species numbers labeled as in Figure 5.

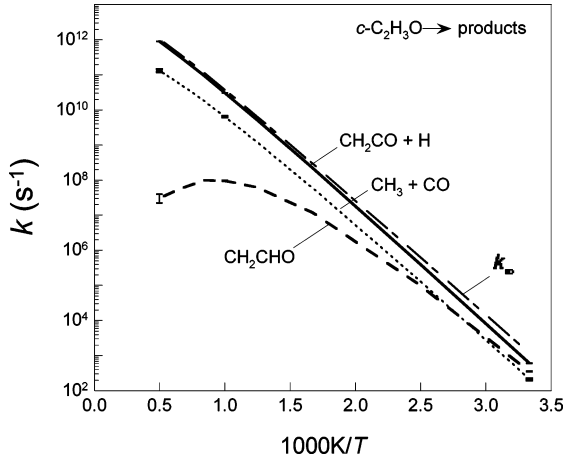

Figure 6. Rate coefficients computed for unimolecular isomerization and decomposition of the oxiranyl radical as a function of temperature (P = 2 atm, M = Ar, and $\langle E_{down} \rangle$ = 260 cm^{-1}). Error bars represent one standard deviation.

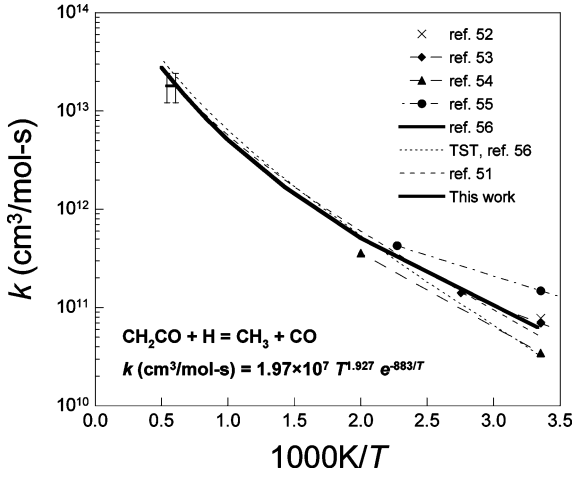

Figure 7. Comparison of rate coefficient computed for $CH_2CO + H \rightarrow CH_3 + CO$ as a function of temperature with experimental data[52−56] and previous theoretical calculations.[51,56] The pressure dependence of the rate coefficient is found to be negligible.

the rates calculated for reactions 1−3, other ethylene oxide reactions whose rate parameters were either taken from literature or estimated, and the detailed reaction mechanism discussed previously. The H-catalyzed isomerization of ethylene oxide to acetaldehyde,

$$c\text{-}C_2H_4O + H \rightarrow CH_3CHO + H \qquad \text{(R4)}$$

had to be added to correctly predict the observed acetaldehyde profiles. Such reactions are definitely not new. A recent study of the H + *c*-C_3H_6 reaction[57] is such an example. Again we obtained the B3LYP/6-31G(d) energy barriers for the concerted H-addition/ring opening process and the subsequent formation of acetaldehyde from the adduct. We calculated the rate coefficient to be

$$k_4\ (cm^3/mol{\cdot}s) = (5.55 \times 10^{13})e^{-5510/T}$$

$$\text{for } 300 \le T \le 2000\ K$$

at 2 atm argon pressure.

The simulation results are compared to experimental data for the thermal decomposition of ethylene oxide in a single-pulse

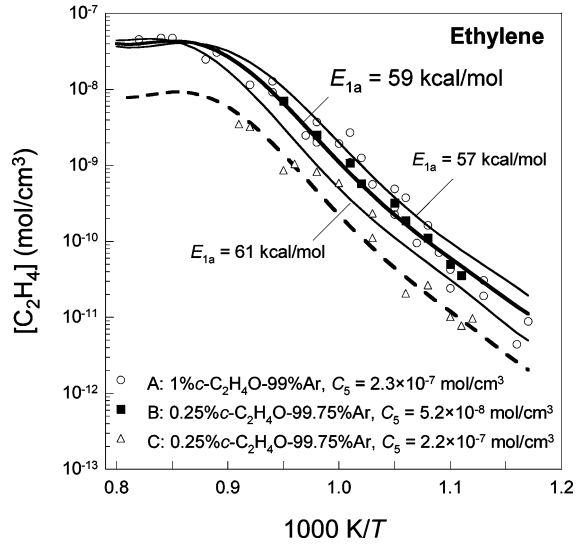

Figure 8. Comparison of predicted (lines) and experimental (symbols, ref 8) concentration profile of ethylene during shock tube pyrolysis of ethylene oxide (dwell time = 2 ms). Computations were carried out for Mixture A (solid lines) and Mixture C (dashed lines).

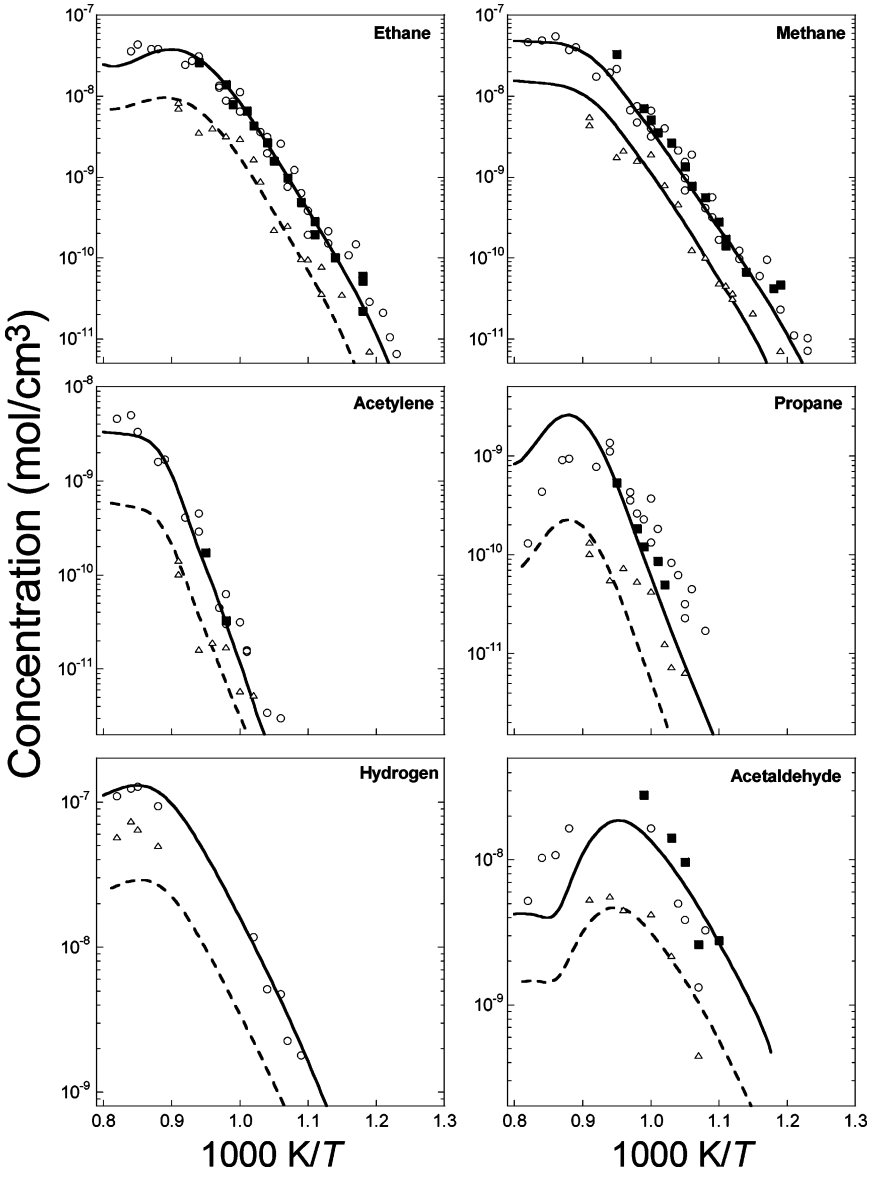

Figure 9. Comparison of predicted (lines) and experimental (symbols, ref 8) concentration profiles of ethane, methane, acetylene, propane, hydrogen, and acetaldehyde during shock tube pyrolysis of ethylene oxide (dwell time = 2 ms). See Figure 8 and its caption for experimental and computational mixture compositions and shock conditions.

shock tube at a dwell time of 2 ms,[8] as seen in Figures 8 and 9. The agreement between the predicted and experimental profiles is satisfactory for all species. The computed concentration profiles do not exhibit pressure dependence, comparing Mixtures A and B, in which the total pressures differ by a factor of ~5, but the initial concentrations of *c*-C_2H_4O are nearly identical. Figure 10 presents ranked sensitivity coefficients for selected species, computed for Mixture A at 1000 K. All of the concentration profiles are the most sensitive to reaction 1b, usually by several factors, compared to secondary reactions. Figure 8 also demonstrates the sensitivity of the ethylene concentration profile with respect to the critical energy chosen for the isomerization of ethylene oxide to acetaldehyde, E_{1a}. From the nominal case with $E_{1a} = 59$ kcal/mol, an increase or decrease in E_{1a} by 2 kcal/mol causes the ethylene concentration to decrease or increase by a factor of ~2, respectively, which approximately encompassed the data scatter over the entire range of temperature. This same level of sensitivity applies to species shown in Figure 9.

Initial radical pool is established through reaction 1b, in accordance with the Rice−Herzfeld mechanism.[58] The further decomposition of ethylene oxide proceeds mainly through H-abstraction by H, OH, and CH_3 radicals to form the oxiranyl radical. For this reason, coupled kinetic uncertainties do exist in k_1, in that most of the species concentrations are affected by the uncertainty in the rate constant of secondary reactions, including reaction 4,

$$CH_3 + H \rightarrow CH_4$$

$$CH_3 + CH_3 \rightarrow C_2H_6$$

and

$$C_2H_6 + H \rightarrow C_2H_5 + H_2$$

Discussion

It has been demonstrated that the species profiles observed during the pyrolysis of ethylene oxide can be reproduced by the current mechanism, assuming an energy barrier $E_{1a} = 59 \pm 2$ kcal/mol for the isomerization of ethylene oxide to form acetaldehyde. The barrier height calculated (Table 4) using the

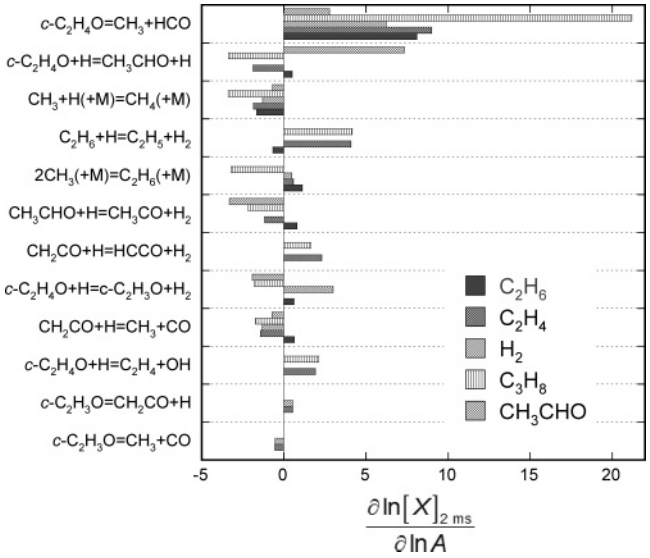

Figure 10. Ranked sensitivity spectra computed for Mixture A at 1000 K (see the caption of Figure 8).

approximate spin-corrected procedure compares favorably to that invoked in the modeling work. Despite attempts in this study to narrow the uncertainty in the calculated isomerization barrier height, a large scatter exists in the SCE values with various basis sets. It should be noted that we have computed the energies of the singlet biradicals using the spin-correction procedure for all steps of the G3 method, except for the step involving the MP2(FU)/G3large method. We find that the energies obtained by single-point calculations using the MP2(FU)/G3large method collapse to the closed-shell singlet, despite using the wave function generated by the calculation on the triplet state. Future work, directed toward the development of theoretical methods to calculate the energies of singlet biradicals and the related energy barriers, is highly desired to treat such systems.

The present work constitutes a step forward in our understanding of the singlet manifold of the C_2H_4O potential energy surface. Combining this singlet PES with that of the triplet states is required to address the chemistry of the $O + C_2H_4$ reaction. This combination of the surfaces requires calculations of the spin−orbit coupling between the singlet and triplet ring-opened $^{\bullet}CH_2CH_2O^{\bullet}$ biradicals. We are hopeful that, with the singlet surface now well defined, we will be able to accurately predict the branching rations and the respective rate constants for the reaction of $O + C_2H_4$.

Thermal rate constants were calculated at pressures of 0.1, 1, and 10 atm. It was found that channel 1a is increasingly important at higher pressures, with the branching ratio at 1000 K increasing from 0.7% at 0.1 atm to 4.6% at 1 atm and 22.3% at 10 atm. Accordingly, the branching ratio of channel 1b reduces from 95.1% at 0.1 atm to 90.6% at 1 atm and 71.7% at 10 atm. The branching ratio of channel 1c is relatively unaffected by the variation of pressure in this range, decreasing slightly from 0.9% at 0.1 atm to 0.8% at 10 atm, at 1000 K. Likewise, the branching ratios of the other channels are relatively insensitive to pressure variations. At 1500 K, the branching ratio for channel 1a increases from 0.04 at 0.1 atm to 0.3% at 1 atm to 2.1% at 10 atm, the branching ratio for channel 1b decreases from 94.5% at 0.1 atm to 93.3% at 1 atm to 90.9% at 10 atm, while again the branching ratio for channel 1c remains almost unchanged, from 1% at 0.1 atm to 1.2% at 10 atm.

Summary

The unimolecular decomposition of ethylene oxide and the oxiranyl radical is examined by molecular orbital calculations, RRKM/Master Equation analysis, and detailed kinetic modeling of ethylene oxide pyrolysis in a single pulse shock tube. The results show that the pyrolysis data are satisfactorily reproduced with an energy barrier height $E_{1a} = 59 \pm 2$ kcal/mol for the isomerization of ethylene oxide to form acetaldehyde. In a very recent independent study, Nguyen et al.[59] reported a similar barrier for this process, confirming our results.

The complexity of the electronic structure of the biradical intermediate, and the transition states associated with it, makes the quantitative calculation of barrier heights highly uncertain. While the spin-correction procedure is a rather crude approximation, it appears to perform quite well and is clearly a significant improvement from the restricted wave functions. We are hopeful that more sophisticated calculations will confirm the applicability of the spin-corrected energies that were rather empirically employed in the current work.

Acknowledgment. This work was supported by AFOSR (Grant No. FA9550-05-1-0010) and by NSF (Grant No. CTS-9874768).

References and Notes

(1) Heckert, W. H.; Mack, E., Jr. *J. Am. Chem. Soc.* **1929**, *51*, 2706.
(2) Mueller, K. H.; Walters, W. P. *J. Am. Chem. Soc.* **1951**, *73*, 1458.
(3) Lossing, F. P.; Ingold, K. J.; Tichnor, A. W. *Discuss. Faraday Soc.* **1953**, *14*, 34.
(4) Mueller, K. H.; Walters, W. P. *J. Am. Chem. Soc.* **1954**, *76*, 330.
(5) Crocco, L.; Glassman, I.; Smith I. E. *J. Chem. Phys.* **1959**, *31*, 506.
(6) Benson S. W. *J. Chem. Phys.* **1964**, *40*, 105.
(7) Setser, D. W. *J. Phys. Chem.* **1966**, *70*, 826.
(8) Lifshitz A.; Ben-Hamou H. *J. Phys. Chem.* **1983**, *87*, 1782.
(9) Kern, R. D.; Singh, H. J.; Xie, K. *17th International Symposium on Shock Waves and Shock Tubes*; Bethlehem, PA, 1989; p 487.
(10) Burcat, A. *Comb. Sci. Technol.* **1980**, *21*, 169.
(11) Würmel, J.; McGuinness, M.; Simmie J. M. *J. Chem. Soc., Faraday Trans.* **1996**, *92*, 715.
(12) Yoon, H. M.; Yeo, H. G.; Yun, S. S.; Kim, C. S.; Kang, J. G. *Combust. Flame* **1993**, *92*, 481.
(13) Kang, J. G.; Ryu, J. C.; Choi, E. S.; Kang, S. K.; Yeo, H. G. *Combust. Flame* **1996**, *106*, 81.
(14) Dagaut, P.; Voisin, D.; Cathonnet, M.; McGuinness, M.; Simmie J. M. *Combust. Flame* **1996**, *106*, 62.
(15) Wesdemiotis, C.; Leyh, B.; Fura, A.; McLafferty, F. W. *J. Am. Chem. Soc.* **1990**, *112*, 8655.
(16) Belbruno, J. J. *J. Phys. Org. Chem.* **1997**, *10*, 113.
(17) Yadav, J. S.; Goddard, J. D. *J. Chem. Phys.* **1986**, *85*, 3975.
(18) Smith, B. J.; Nguyen, M. T.; Bouma, W. J.; Radom, L. *J. Am. Chem. Soc.* **1991**, *113*, 6452.
(19) Yadav, J. S.; Goddard, J. D. *J. Chem. Phys.* **1986**, *84*, 2682.
(20) Martell, J. M.; Yu, H.; Goddard, J. D. *Mol. Phys.* **1997**, *92*, 497.
(21) Gherman, B. F.; Friesner, R. A.; Wong, T.-H.; Min Z.; Bersohn, R. *J. Chem. Phys.* **2001**, *114*, 6128.
(22) Bigot B.; Sevin, A.; Devaquet, A. *J. Am. Chem. Soc.* **1979**, *101*, 1095.
(23) Yamaguchi, K.; Yabushita S.; Fueno, T.; Kato, S.; Morokuma, K. *Chem. Phys. Lett.* **1980**, *70*, 27.
(24) Dupuis, M.; Wendoloski, J. J.; Takada, T.; Lester, W. A., Jr. *J. Chem. Phys.* **1982**, *76*, 481.
(25) Fueno, T.; Takahara, Y.; Yamaguchi, K. *Chem. Phys. Lett.* **1990**, *167*, 291.
(26) Roszak, S.; Buenker, R. J.; Hariharan, P. C.; Kaufman, J. J. *Chem. Phys.* **1990**, *147*, 13.
(27) Knuts, S.; Minaev, B. F.; Vahtras, O.; Ågren, H. *Int. J. Quantum Chem.* **1995**, *55*, 23.
(28) Frisch, M. J.; Trucks, G. W.; Schlegel, H. B.; Scuseria, G. E.; Robb, M. A.; Cheeseman, J. R.; Montgomery, J. A., Jr.; Vreven, T.; Kudin, K. N.; Burant, J. C.; Millam, J. M.; Iyengar, S. S.; Tomasi, J.; Barone, V.; Mennucci, B.; Cossi, M.; Scalmani, G.; Rega, N.; Petersson, G. A.; Nakatsuji, H.; Hada, M.; Ehara, M.; Toyota, K.; Fukuda, R.; Hasegawa, J.; Ishida, M.; Nakajima, T.; Honda, Y.; Kitao, O.; Nakai, H.; Klene, M.; Li, X.; Knox, J. E.; Hratchian, H. P.; Cross, J. B.; Bakken, V.; Adamo, C.;

Jaramillo, J.; Gomperts, R.; Stratmann, R. E.; Yazyev, O.; Austin, A. J.; Cammi, R.; Pomelli, C.; Ochterski, J. W.; Ayala, P. Y.; Morokuma, K.; Voth, G. A.; Salvador, P.; Dannenberg, J. J.; Zakrzewski, V. G.; Dapprich, S.; Daniels, A. D.; Strain, M. C.; Farkas, O.; Malick, D. K.; Rabuck, A. D.; Raghavachari, K.; Foresman, J. B.; Ortiz, J. V.; Cui, Q.; Baboul, A. G.; Clifford, S.; Cioslowski, J.; Stefanov, B. B.; Liu, G.; Liashenko, A.; Piskorz, P.; Komaromi, I.; Martin, R. L.; Fox, D. J.; Keith, T.; Al-Laham, M. A.; Peng, C. Y.; Nanayakkara, A.; Challacombe, M.; Gill, P. M. W.; Johnson, B.; Chen, W.; Wong, M. W.; Gonzalez, C.; Pople, J. A. *Gaussian03*; Gaussian, Inc.: Wallingford, CT, 2004.

(29) Stephens, P. J.; Devlin, F. J.; Chablowski, C. F.; Frisch, M. J. *J. Phys. Chem.* **1994**, *98*, 11623.

(30) (a) Becke, A. D. *J. Chem. Phys*. **1992**, *97*, 9173. (b) Becke, A. D. *J. Chem. Phys*. **1993**, *98*, 5648.

(31) Lee, C.; Yang, W.; Parr, R. G. *Phys. Rev.* **1988**, *B37*, 785.

(32) Baboul, A. G.; Larry C. A.; Redfern, P. C.; Raghavachari K. *J. Chem. Phys*. **1999**, *110*, 7650.

(33) Peng, C.; Schlegel, H. B. *Isr. J. Chem.* **1993**, *33*, 449.

(34) (a) Gonzalez, C.; Schlegel, H. B. *J. Chem. Phys*. **1989**, *90*, 2154. (b) Gonzalez, C.; Schlegel, H. B. *J. Chem. Phys*. **1990**, *94*, 5523.

(35) Yamaguchi, K.; Jensen, F.; Dorigo, A.; Houk, K. N. *Chem. Phys. Lett.* **1988**, *149*, 537.

(36) Shao, Y.; Head-Gordon, M.; Krylov, A. I. *J. Chem. Phys.* 2003, **118**, 4807.

(37) Holbrook, K. A.; Pilling, M. J.; Robertson, S. H. *Unimolecular Reactions*, 2nd ed.; Wiley: Chichester, UK, 1996.

(38) Gilbert, R. G.; Smith, S. C. *Theory of Unimolecular and Recombination Reactions*; Blackwell-Scientific: Oxford, UK, 1990.

(39) (a) Whitten, G. Z.; Rabinovitch, B. S. *J Chem. Phys*. **1963**, *38*, 2466. (b) Whitten, G. Z.; Rabinovitch, B. S. *J Chem. Phys*. **1964**, *41*, 1883.

(40) Astholz, D. C.; Troe, J.; Wieters, W. J. *J. Chem. Phys.* **1979**, *70*, 5107.

(41) Joshi, A. V.; Wang H. Master equation modeling of wide temperature and pressure dependence of CO + OH → products. *Int. J. Chem. Kinet.* **2004**, submitted for publication.

(42) Kee, R. J.; Rupley, F. M.; Miller, J. A. Sandia Report SAND 89-8009B; Sandia National Laboratories: Albuquerque, NM, 1989.

(43) Davis, S. G.; Joshi, A. V.; Wang, H.; Egolfopoulos, F. *Proceedings of the 30th Symposium* (*International*) *on Combustion*; The Combustion Institute: Pittsburgh, PA, 2004; p 1283.

(44) Frenklach, M.; Wang, H.; Goldenberg, M.; Smith, G. P.; Golden, D. M.; Bowman, C. T.; Hanson, R. K.; Gardiner, W. C.; Lissiansky, V. GRI-Mech: An Optimized Chemical Reaction Mechanism for Methane Combustion (version GRI-Mech 1.2), GRI Report No. GRI-95/0058; Gas Research Institute: Chicago, IL, 1995.

(45) Davis, S. G.; Law, C. K.; Wang, H. *27th Symposium (International) on Combustion*; The Combustion Institute: Pittsburgh, PA, 1998; p 305.

(46) Davis, S. G.; Law, C. K.; Wang, H. *J. Phys. Chem. A* **1999**, *103*, 5889.

(47) Davis, S. G.; Law, C. K.; Wang, H. *Combust. Flame* **1999**, *119*, 375.

(48) Bogan, D. J.; Hand, C. W. *J. Phys. Chem.* **1978**, *82*, 2067.

(49) Baldwin, R. R.; Keen, A.; Walker, R. W. *J. Chem. Soc., Faraday Trans.* **1984**, *80*, 435.

(50) Wesdemiotis, C.; McLafferty, F. W. *J. Am. Chem. Soc*. **1987**, *109*, 4760.

(51) Lee, J.; Bozzelli, J. W. *Int. J. Chem. Kinet.* **2003**, *35*, 20.

(52) Carr, R. W., Jr.; Gay, I. D.; Glass, G. P.; Niki, H. *J. Chem. Phys.* **1968**, *49*, 846.

(53) Slemr, F.; Warneck, P. *Ber. Bunsen-Ges. Phys. Chem.* **1975**, *79*, 152.

(54) Michael, J. V.; Nava, D. F.; Payne, W. A.; Stief, L. J. *J. Chem. Phys.* **1979**, *70*, 5222.

(55) Umemoto, H.; Tsunashima, S.; Sato, S.; Washida, N.; Hatakeyama, S. *Bull. Chem. Soc. Jpn.* **1984**, *57*, 2578.

(56) Frank, P.; Bhaskaran, K. A.; Just, Th. *J. Phys. Chem.* **1986**, *90*, 2226.

(57) Yu, H.-G.; Muckerman, J. T. *J. Phys. Chem.* **2004**, *108*, 10844.

(58) Rice, F. O.; Herzfeld, K. F. *J. Am. Chem. Soc.* **1934**, *56*, 284.

(59) Nguyen, T. L.; Vereecken, V.; Hou, X. J.; Nguyen, M. T.; Peeters, J. *J. Phys. Chem. A* **2005**, *109*, 7489.